Rigorous Boundary Integral Equation Solution for General Isotropic and Uniaxial Anisotropic Dielectric Waveguides in Multilayered Media Including Losses, Gain and Leakage

Frank Olyslager, *Student Member, IEEE,* and Daniël De Zutter, *Member, IEEE*

Abstract—**Bounded and leaky eigenmodes of arbitrary shaped polygonal dielectric waveguides embedded in a multilayered medium are determined based on a rigorous full-wave analysis. The dielectric waveguides consist of isotropic or uniaxial anisotropic material. Losses and gain inside the layers and the waveguides are allowed. The eigenmodes are determined with a boundary integral equation technique in conjunction with the method of moments. Results for the propagation constants are presented for a number of waveguides and, where possible, compared with published data. Special attention is devoted to the transition from a dielectric waveguide to a perfectly conducting waveguide when the loss tangent of the waveguide material changes from zero to infinity.**

I. Introduction

In [1] and [2] a rigorous analysis of the propagation characteristics of general lossless and lossy multiconductor transmission lines in multilayered media was presented. In this contribution, the authors would like to extend the technique presented in [1] and [2] to dielectric waveguides. The boundary integral equation presented in [1] is extended to uniaxial anisotropic waveguides with the optical axes along the propagation direction. The method of moment Galerkin solution technique of the integral equation is the same as in [1] and will not be repeated in detail here.

Dielectric waveguides have been investigated by a large number of authors, using a multitude of different methods. We will restrict ourselves to giving a short overview of the most important analysis techniques and discuss the properties of our technique compared to these techniques. A more extensive discussion of various techniques can be found in the Introduction of [3] and in [4] where a number of different techniques were used to analyze optical waveguides.

Several authors used the mode-matching technique to analyze open and closed dielectric waveguide structures. However, these methods are restricted to waveguides consisting of piecewise rectangular homogeneous regions. Finite element (FEM) and finite difference methods (FDM), used for example in [5], allow inhomogeneous regions but do not incorporate leakage. The finite difference time domain (FDTD) and the transmission line method (TLM) suffer from the lack of accurate absorbing boundary conditions and are not very suited for frequency domain calculations with frequency-dependent material parameters and to handle losses due to the skin effect. Dielectric waveguides in multilayered media have also been analyzed with good success with domain integral equation (DIE) techniques [3], [6]. In [3] and [6] a method of moments technique combined with Galerkin is used. This technique is very suitable to analyze inhomogeneous waveguides because in the moment method the cross-section of the waveguide is divided into a mesh of small cells. In [3] only results for waveguides with homogeneous rectangular cross section are presented.

Our boundary integral equation (BIE) technique only requires the discretization of the boundary of the waveguide. This has several advantages over the DIE methods. The number of unknowns and the size of the final system-matrix is drastically reduced because only a one-dimensional (1-D) boundary has to be discretized instead of a two-dimensional (2-D) cross-section. In DIE methods, dielectric waveguides with skew boundaries require the refinement of the mesh in order to accurately describe the boundary. This increases the number of unknowns. The mesh also has to be refined when losses become important in order to accurately represent the rapid field changes due to the skin effect. The same 2-D mesh problems also arise in FEM, FDM, FDTD, and TLM methods. In the BIE technique, no increase of the number of discretizations is necessary for skew sides or losses. On the other hand, the BIE technique is not suited to analyze waveguides with inhomogeneous cross-sections. This would require the division of the waveguide into a number of homogeneous regions and the discretization of all the boundaries of these regions would result in a large number of unknowns.

After a description of the geometry and the notations adopted in this paper, the authors start their discussion with the construction of the BIE for anisotropic waveguides. Though the theory is valid for arbitrary shaped waveguides, as in [1], the authors restrict themselves to polygonal waveguides. In the example, the authors will show that curved waveguides are accurately approximated by polygonal boundaries. After the construction of the BIE, the authors will give a short

Manuscript received July 13, 1992; revised January 12, 1993.

The authors are with the Laboratory of Electromagnetism and Acoustics, University of Ghent, 9000 Ghent, Belgium and also with the National Fund for Scientific Research, Belgium.

IEEE Log Number 9210227.

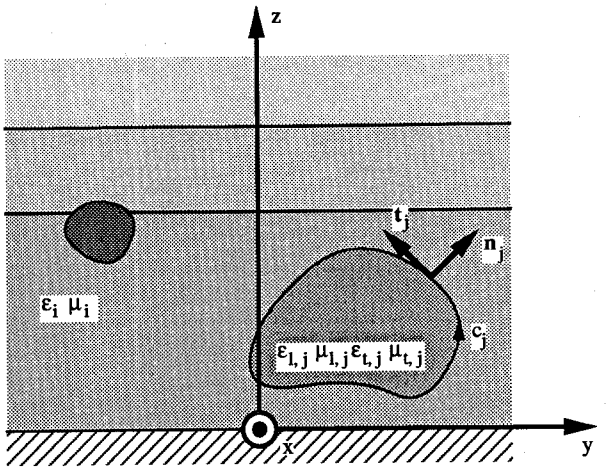

Fig. 1. Geometry of general coupled dielectric waveguides in a multilayered medium.

overview of its solution technique. In this paper, attention will be focused on the examples. Examples with losses, gain, anisotropy, and very general cross-sections are presented and where possible compared with analytical results and results in [3]. To the authors knowledge, it is the first time that the change in behavior from a pure dielectric waveguide, embedded in a multilayered medium, to a perfectly conducting one, by gradually increasing the conductivity is analyzed.

The authors finally would like to emphasize that with the term "dielectric waveguide" they only mean the local disturbance of the layered medium and not the whole layered structure including that disturbance.

II. Geometry of the Problem

Fig. 1 shows the geometry of the analyzed structures. There are L layers and the authors will use the subscript $i\,(i = 1, 2, \cdots, \mathrm{L})$ to refer to the ith layer. Each layer consists of homogeneous and isotropic material characterized by an arbitrary complex permittivity ε_i and complex permeability μ_i.

A total number of W waveguides are embedded in the layered medium and the subscript j, $(j = 1, 2, \cdots, \mathrm{W})$ refers to the jth waveguide. Because a waveguide can be located in more than one layer we use the notation W_i to indicate the total number of waveguides in layer i while the subscript i_j, $(j = 1, 2, \cdots, \mathrm{W}_i)$ refers to the i_jth waveguide in layer i.

Each waveguide j consists of homogeneous and anisotropic material characterized by a permittivity tensor $\overline{\varepsilon}_j$ and permeability tensor $\overline{\mu}_j$ which take the following form in the coordinate system of Fig. 1:

$$\overline{\varepsilon}_j = \begin{vmatrix} \varepsilon_{l,j} & 0 & 0 \\ 0 & \varepsilon_{t,j} & 0 \\ 0 & 0 & \varepsilon_{t,j} \end{vmatrix} \qquad \overline{\mu}_j = \begin{vmatrix} \mu_{l,j} & 0 & 0 \\ 0 & \mu_{t,j} & 0 \\ 0 & 0 & \mu_{t,j} \end{vmatrix} \tag{1}$$

$\varepsilon_{l,j}$, respectively, $\varepsilon_{t,j}$ and $\mu_{l,j}$, respectively, $\mu_{t,j}$ are the longitudinal, respectively, transversal complex permittivity and permeability. The boundary of waveguide j is denoted by c_j. Note that c_{i_j} is the boundary of the i_jth waveguide in layer i. $\boldsymbol{n}_j$ is the external normal to c_j and $\boldsymbol{r}_j(y, z)$ is the position vector in the (y, z) plane of a point on c_j.

III. Construction of the Integral Equation

A. Introduction

The common time and longitudinal dependence $e^{j(\omega t - \beta x)}$ in all field components, with ω the pulsation and β the complex propagation constant, is omitted. As in [1], the unknown sources of the integral equation are the tangential fields $\boldsymbol{n}_j \times \boldsymbol{E}(\boldsymbol{r}_j)$ and $\boldsymbol{n}_j \times \boldsymbol{H}(\boldsymbol{r}_j)$ at the boundaries of the waveguides. These tangential fields consist of components in the cross-section $E_t(\boldsymbol{r}_j)$, $H_t(\boldsymbol{r}_j)$ and longitudinal components $E_x(\boldsymbol{r}_j)$, $H_x(\boldsymbol{r}_j)$. The electromagnetic fields inside and outside the waveguides are expressed as contour integrals along the boundaries of the waveguides as function of the unknown sources. The final integral equation is found by imposing the continuity of the tangential fields at the boundaries of the waveguides.

B. Inside a Waveguide

Consider waveguide j at the right side of Fig. 1 with boundary c_j consisting of homogeneous uniaxial anisotropic material. Elimination of E_y, E_z, H_y, and H_z in Maxwell's equations results in the following Helmholtz equation for E_x:

$$\frac{\partial^2 E_x}{\partial y^2} + \frac{\partial^2 E_x}{\partial z^2} + \gamma_{E,j}^2 E_x = 0$$
$$\gamma_{E,j}^2 = \omega^2 \varepsilon_{l,j} \mu_{t,j} - \beta^2 \frac{\varepsilon_{l,j}}{\varepsilon_{t,j}}. \tag{2}$$

For H_x one obtains an analogous equation as follows:

$$\frac{\partial^2 H_x}{\partial y^2} + \frac{\partial^2 H_x}{\partial z^2} + \gamma_{H,j}^2 H_x = 0$$
$$\gamma_{H,j}^2 = \omega^2 \mu_{l,j} \varepsilon_{t,j} - \beta^2 \frac{\mu_{l,j}}{\mu_{t,j}}. \tag{3}$$

More general anisotropic permittivity and permeability tensors do not result in simple Helmholtz differential equations for the longitudinal field components.

As is explained in [1], using Green's identity and the coordinate system $(\boldsymbol{t}_j, \boldsymbol{n}_j)$ of Fig. 1, it can be shown that the longitudinal field components inside the waveguide can be expressed as a contour integral along the boundary c_j

$$E_{x,j}(\boldsymbol{r}) = \oint_{c_j} \left[E_{x,j} \frac{\partial G_{E,j}}{\partial n_j'} - G_{E,j} \frac{1}{\omega \varepsilon_{t,j}} \cdot \left(-\beta \frac{\partial H_{x,j}}{\partial t_j'} + j \gamma_{t,j}^2 H_{t,j} \right) \right] dc'$$
$$H_{x,j}(\boldsymbol{r}) = \oint_{c_j} \left[H_{x,j} \frac{\partial G_{H,j}}{\partial n_j'} - G_{H,j} \frac{1}{\omega \mu_{t,j}} \cdot \left(\beta \frac{\partial E_{x,j}}{\partial t_j'} - j \gamma_{t,j}^2 E_{t,j} \right) \right] dc' \tag{4}$$

with $\gamma_{t,j}^2 = \omega^2 \varepsilon_{t,j} \mu_{t,j} - \beta^2$ and with $G_{E,j}(\boldsymbol{r} \mid \boldsymbol{r}')$ and $G_{H,j}(\boldsymbol{r} \mid \boldsymbol{r}')$ the 2-D homogeneous space Green's functions of the Helmholtz equations (2) and (3)

$$G_{E,j}(\boldsymbol{r} \mid \boldsymbol{r}') = \frac{j}{4} H_0^{(2)}(\gamma_{E,j} |\boldsymbol{r} - \boldsymbol{r}'|)$$
$$G_{H,j}(\boldsymbol{r} \mid \boldsymbol{r}') = \frac{j}{4} H_0^{(2)}(\gamma_{H,j} |\boldsymbol{r} - \boldsymbol{r}'|). \tag{5}$$

$H_0^{(2)}$ is the Hankel function of the second kind and zeroth order. From (4), it follows that $E_{x,j}(\boldsymbol{r})$ and $H_{x,j}(\boldsymbol{r})$ are fully determined in every point $\boldsymbol{r}$ inside c_j if $E_{x,j}$, $H_{x,j}$, $E_{t,j}$, and $H_{t,j}$ and hence $\partial E_{x,j}/\partial t$ and $\partial H_{x,j}/\partial t$ are known on the boundary c_j.

C. Outside The Waveguides

In [1] the authors obtained the following expressions for the longitudinal fields inside layer i outside the waveguides:

$$E_{x,i}(\boldsymbol{r}) = \sum_{i_j=1}^{W_i} E_{x,i_j}^{\text{in}}(\boldsymbol{r}) + \sum_{j=1}^{W} E_{x,i}^{\text{sc}}(\boldsymbol{r});$$
$$H_{x,i}(\boldsymbol{r}) = \sum_{i_j=1}^{W_i} H_{x,i_j}^{\text{in}}(\boldsymbol{r}) + \sum_{j=1}^{W} H_{x,i}^{\text{sc}}(\boldsymbol{r}). \tag{6}$$

E_{x,i_j}^{in} and H_{x,i_j}^{in} are the longitudinal incoming field components generated by the i_jth waveguide in layer i as if this layer fills up whole space. These field components are given by the following:

$$E_{x,i_j}^{\text{in}}(\boldsymbol{r}) = -\oint_{c_{i_j}} \left[E_{x,i_j} \frac{\partial G_i}{\partial n'_{i_j}} - G_i \frac{1}{\omega\varepsilon_i} \cdot \left(-\beta \frac{\partial H_{x,i_j}}{\partial t_{i_j}} + j\gamma_i^2 H_{t,i_j} \right) \right] dc'$$
$$H_{x,i_j}^{\text{in}}(\boldsymbol{r}) = -\oint_{c_{i_j}} \left[H_{x,i_j} \frac{\partial G_i}{\partial n'_{i_j}} - G_i \frac{1}{\omega\mu_i} \cdot \left(\beta \frac{\partial E_{x,i_j}}{\partial t'_{i_j}} - j\gamma_i^2 E_{t,i_j} \right) \right] dc' \tag{7}$$

with

$$G_i(\boldsymbol{r} \mid \boldsymbol{r}') = \frac{j}{4} H_0^{(2)}(\gamma_i|\boldsymbol{r} - \boldsymbol{r}'|) \qquad \gamma_i^2 = \omega^2\varepsilon_i\mu_i - \beta^2. \tag{8}$$

Remark the resemblance with (4). $E_{x,i}^{\text{sc}}$ and $H_{x,i}^{\text{sc}}$ in (6) are the longitudinal scattered field components who find their origin in the scattering in the layered medium of the incoming fields generated by waveguide i. The authors refer the reader to [1], [2], or [7] for a discussion of the determination of the scattered fields.

D. The Final Integral Equation

As mentioned above the final integral equation, or more correct the coupled set of integral equations, is obtained by imposing the continuity of the integral representations of the tangential field components inside and outside the waveguide at the waveguide boundaries:

$$\lim_{r\to r_{i_o}} \left[\sum_{i_j=1}^{W_i} E_{x,i_j}^{\text{in}}(\boldsymbol{r}) + \sum_{j=1}^{W} E_{x,i}^{\text{sc}}(\boldsymbol{r}) \right] = \lim_{r\to r_{i_o}} E_{x,o}(\boldsymbol{r})$$
$$\lim_{r\to r_{i_o}} \left[\sum_{i_j=1}^{W_i} H_{x,i_j}^{\text{in}}(\boldsymbol{r}) + \sum_{j=1}^{W} H_{x,i}^{\text{sc}}(\boldsymbol{r}) \right] = \lim_{r\to r_{i_o}} H_{x,o}(\boldsymbol{r})$$
$$\lim_{r\to r_{i_o}} \left[\sum_{i_j=1}^{W_i} \left(\frac{j\omega\mu_i}{\gamma_i^2} \frac{\partial H_{x,i_j}^{\text{in}}}{\partial n} - \frac{j\beta}{\gamma_i^2} \frac{\partial E_{x,i_j}^{\text{in}}}{\partial t} \right) + \sum_{j=1}^{W} \left(\frac{j\omega\mu_i}{\gamma_i^2} \frac{\partial H_{x,j}^{\text{sc}}}{\partial n} - \frac{j\beta}{\gamma_i^2} \frac{\partial E_{x,j}^{\text{sc}}}{\partial t} \right) \right]$$
$$= \lim_{r\to r_{i_o}} \left(\frac{j\omega\mu_{t,o}}{\gamma_{t,o}^2} \frac{\partial H_{x,o}^{\text{in}}}{\partial n} - \frac{j\beta}{\gamma_{t,o}^2} \frac{\partial E_{x,o}^{\text{in}}}{\partial t} \right)$$
$$\lim_{r\to r_{i_o}} \left[\sum_{i_j=1}^{W_i} \left(-\frac{j\omega\varepsilon_i}{\gamma_i^2} \frac{\partial E_{x,i_j}^{\text{in}}}{\partial n} - \frac{j\beta}{\gamma_i^2} \frac{\partial H_{x,i_j}^{\text{in}}}{\partial t} \right) + \sum_{j=1}^{W} \left(-\frac{j\omega\varepsilon_i}{\gamma_i^2} \frac{\partial E_{x,j}^{\text{sc}}}{\partial n} - \frac{j\beta}{\gamma_i^2} \frac{\partial H_{x,j}^{\text{sc}}}{\partial t} \right) \right]$$
$$= \lim_{r\to r_{i_o}} \left(\frac{j\omega\varepsilon_{t,o}}{\gamma_{t,o}^2} \frac{\partial E_{x,o}^{\text{in}}}{\partial n} - \frac{j\beta}{\gamma_{t,o}^2} \frac{\partial H_{x,o}^{\text{in}}}{\partial t} \right) \tag{9}$$

with $i_o = 1, 2, \cdots, W_i$ and $i = 1, 2, \cdots, L$. r_{i_o} represents a point on boundary c_{i_o}. The subscript o in the fields at the right-hand side of (9) refers to the waveguide to which c_{i_o} belongs. At the left-hand side of (9), the limit is taken from outside boundary c_{i_o} while at the right-hand side the limit is taken from the inside. This homogeneous set of integral equations will only have non-trivial solutions for discrete values of the propagation constant β.

IV. Numerical Solution

The detailed solution technique of the integral equation is presented in [1]. Here the authors will present a short overview of this technique and restrict themselves to results needed in Section V.

This set of integral equations is solved numerically with a Galerkin method of moments. For this purpose the polygonal boundaries of the waveguides are divided into a number of segments. The unknown longitudinal field components $E_{x,j}(\boldsymbol{r}_j)$ and $H_{x,j}(\boldsymbol{r}_j)$ are expanded in overlapping triangular basis functions. The transversal tangential field components $E_{t,j}(\boldsymbol{r}_j)$ and $H_{t,j}(\boldsymbol{r}_j)$ are expanded in pulse basis functions. In the method of Galerkin we test the first two continuity relations of (9), i.e., the longitudinal field relations, with pulse functions and the last two relations, i.e., the transversal tangential relations with overlapping triangular functions. The integration over the basis functions is called the excitation integration and the observation integration is the integration over the test functions.

In a next step the field components (9) are spatially Fourier transformed and inverse Fourier transformed in the y direction. The inverse Fourier transform is then interchanged with the limit operation and with the observation integration. The remaining Fourier transform on the other hand is interchanged with the excitation integration. This transition to the spatial Fourier domain allows us to perform both the excitation and observation integration analytically because the Fourier transform of the Hankel function appearing in the Green's functions (5) and (8) takes a simple form [8] as follows:

$$\frac{1}{2\pi} \int_{-\infty}^{+\infty} H_0^{(2)}(\gamma|\boldsymbol{r} - \boldsymbol{r}'|) e^{jk_y y}\, dy = \frac{j}{\pi} \frac{e^{jk_y y'} e^{-\Gamma|z-z'|}}{\Gamma}. \tag{10}$$

k_y is the spectral variable and $\Gamma^2 = k_y^2 - \gamma^2$. For the incoming field components on the right- and left-hand side of (9), any other direction in the cross-section than the y direction can be chosen as spatial Fourier transform direction. For the scattered field components on the left-hand side of (9) it is necessary to transform in the y direction. This allows us to determine the transformed scattered fields analytically [1], [2], [7], and [9].

Only the final inverse Fourier transformation has to be determined numerically. This involves an integration over the real axes in the complex k_y plane. Because of the existence of poles and/or branch cuts in the spectral scattered fields it is necessary to deform the integration path into the complex k_y plane. How this is done will be discussed in the next section.

V. Inverse Fourier Integration Path for the Scattered Contributions

The integrand of the final inverse Fourier transform takes the following general form for the scattered contributions in (9):

$$\int_{-\infty}^{+\infty} f(k_y) e^{jk_y \Delta y} e^{-\Gamma|\Delta z|}\, dk_y \tag{11}$$

$f(k_y)$ contains transmission and reflection coefficients of the layered medium and $f(k_y)$ will exhibit poles corresponding to the resonances of the layered medium, i.e., corresponding to the eigenmodes of the layered structure. $f(k_y)$ will also have branch cuts due to the square root in Γ for the Γ's of the semi-infinite layers. It is well known [10] that $f(k_y)$ is an even function of the Γ's of layers with finite thickness. Hence layers with finite thickness will not yield branch cuts. Now the authors will discuss how to maneuver the inverse Fourier transformation integration path through the complex k_y plane.

Consider a mode, with complex propagation constant β, propagating along the lossless structure on the inset of Fig. 2. The propagation constants of the modi above cut off of the layered structure, i.e., the structure of Fig. 2 without the rectangular waveguide, are denoted by $\lambda_k (k = 1, \cdots, K)$. We assume that $\mathrm{Re}(\beta)$ is smaller than some of the λ_k and larger than $k_0 \left(= \omega\sqrt{\varepsilon_0 \mu_0}\right)$. Hence the mode under consideration is a leaky mode which leaks into surface waves in the substrate but not into space waves. The propagation constant of the mode has a positive real part and a negative imaginary part. The spectral function $f(k_y)$ for the scattered field components in (11) has poles at:

$$k_{y,p,k}^{\pm} = \pm\sqrt{\lambda_k^2 - \beta^2} \tag{12}$$

and branch points due to the semi-infinite top layer at:

$$k_{y,b}^{\pm} = \pm\sqrt{k_0^2 - \beta^2}\,. \tag{13}$$

The branch points and the poles are located in the first and third quadrant of the complex plane (Fig. 2). As shown in [11], the authors can, for example, define the branch cuts by $\mathrm{Im}(\Gamma^2) = 0$ and $\mathrm{Re}(\Gamma^2) < 0$. In the complex k_y plane these branch cuts are parts of hyperbolas. In the first quadrant the inverse integration path has to run above the surface wave poles $k_{y,p,k}^{+}$, in order to incorporate leakage in a correct way, without intersecting the branch cut (curve C_1 on Fig. 2) or without circumventing a $k_{y,p,k}^{-}$ pole, with $\lambda_k < \mathrm{Re}(\beta)$, which has migrated from the positive imaginary axes into the first quadrant. However it is allowed to cross the branch cuts but then the part of the integration path between both branch cuts has to be located in the other Riemann plane for which $\mathrm{Re}(\Gamma) < 0$ (curve C_2 on Fig. 2) [12]. If the substrate becomes lossy then λ_k becomes complex with a negative imaginary part. This will also result in an increase of $|\mathrm{Im}(\beta)|$ but that increase will be less prominent. The surface wave poles $k_{y,p,k}^{+}$ in the first quadrant will migrate down and eventually end up in the fourth quadrant.

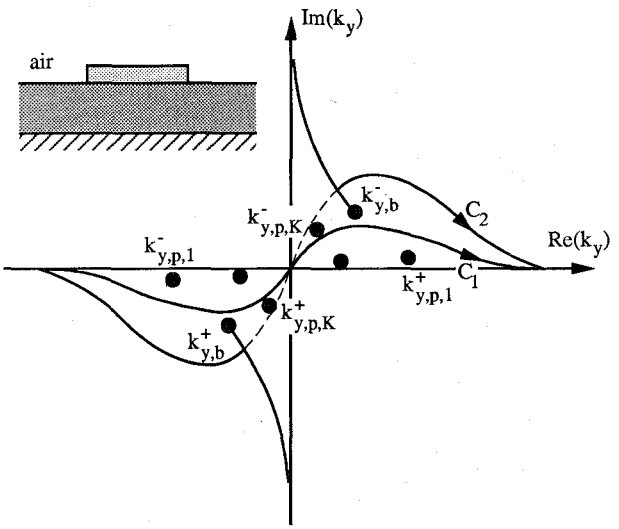

Fig. 2. Inverse Fourier integration path in the complex k_y plane for the scattered field components of the strip dielectric waveguide in the inset.

VI. Case Studies

A. Anisotropic Dielectric Fiber

Consider a homogeneous dielectric fiber with radius a, permittivities $\varepsilon_{t,1}$ and $\varepsilon_{l,1}$ and permeabilities $\mu_{t,1}$ and $\mu_{l,1}$ in an infinite homogeneous space with parameters $\varepsilon_{t,2}$, $\varepsilon_{l,2}$, $\mu_{t,2}$ and $\mu_{l,2}$. In polar coordinates it is easy to analytically determine the equation for the propagation constants of the modi propagating along this structure. If one parallels the derivation presented in [13] for the isotropic case, one obtains the following equation for the anisotropic case:

$$\begin{aligned}\frac{\beta^2 n^2}{\omega^2}\left(\frac{1}{\gamma_{t,1}^2} - \frac{1}{\gamma_{t,2}^2}\right)^2 = &- \frac{\varepsilon_{t,2}\mu_{t,1} u_H w_E}{\gamma_{t,1}^2 \gamma_{t,2}^2} \frac{J_n'(u_H)}{J_n(u_H)} \frac{K_n'(w_E)}{K_n(w_E)} \\ &+ \frac{\varepsilon_{t,2}\mu_{t,2} w_E w_H}{\gamma_{t,2}^4} \frac{K_n'(w_E)}{K_n(w_E)} \frac{K_n'(w_H)}{K_n(w_H)} \\ &- \frac{\varepsilon_{t,1}\mu_{t,2} u_E w_H}{\gamma_{t,1}^2 \gamma_{t,2}^2} \frac{J_n'(u_E)}{J_n(u_E)} \frac{K_n'(w_H)}{K_n(w_H)} \\ &+ \frac{\varepsilon_{t,1}\mu_{t,1} u_E u_H}{\gamma_{t,1}^4} \frac{J_n'(u_E)}{J_n(u_E)} \frac{J_n'(u_H)}{J_n(u_H)}\end{aligned} \tag{14}$$

with

$$u_E = a\gamma_{E,1} = a\sqrt{\omega^2 \varepsilon_{l,1}\mu_{t,1} - \beta^2 \frac{\varepsilon_{l,1}}{\varepsilon_{t,1}}}$$

TABLE I
COMPARISON BETWEEN THE NORMALIZED PROPAGATION CONSTANTS β/k_0 OF THE MODI OF A DIELECTRIC ISOTROPIC AND ANISOTROPIC FIBER APPROXIMATED BY A HEXAGON AND AN OCTAGON AND THE FACT ANALYTICAL RESULTS.

Isotropic dielectric fiber $\varepsilon_{r,t,1} = \varepsilon_{r,l,1} = 2.55$							
	Circular	Hexagon			Octagon		
	analytical solution (14)	2 divisions per side	3 divisions per side	4 divisions per side	2 divisions per side	3 divisions per side	4 divisions per side
HE_{11}	1.40486	1.40418	1.40396	1.40393	1.40464	1.40454	1.40451
TE_{01}	1.18199	1.18299	1.17918	1.17838	1.18195	1.18078	1.18050
TM_{01}	1.10756	1.11141	1.10979	1.10955	1.10862	1.10831	1.10827
HE_{21}	1.08008	1.07708	1.07900	1.07954	1.07892	1.07968	1.07962
Anisotropic dielectric fiber $\varepsilon_{r,t,1} = 2.55$ and $\varepsilon_{r,l,1} = 2.00$							
	Circular	Hexagon			Octagon		
	analytical solution (14)	2 divisions per side	3 divisions per side	4 divisions per side	2 divisions per side	3 divisions per side	4 divisions per side
HE_{11}	1.38340	1.38412	1.38408	1.38409	1.38900	1.38427	1.38426
TE_{01}	1.18199	1.18292	1.17891	1.17808	1.18499	1.18069	1.18038
TM_{01}	1.05390	1.05693	1.05624	1.05620	1.05381	1.05471	1.05473
HE_{21}	1.04531	1.04641	1.04832	1.04882	1.04743	1.04847	1.04867

$$u_H = a\gamma_{H,1} = a\sqrt{\omega^2\mu_{l,1}\varepsilon_{t,1} - \beta^2\frac{\mu_{l,1}}{\mu_{t,1}}}$$
$$w_E = a|\gamma_{E,2}| = a\sqrt{\beta^2\frac{\varepsilon_{l,2}}{\varepsilon_{t,2}} - \omega^2\varepsilon_{l,2}\mu_{t,2}}$$
$$w_H = a|\gamma_{H,2}| = a\sqrt{\beta^2\frac{\mu_{l,2}}{\mu_{t,2}} - \omega^2\mu_{l,2}\varepsilon_{t,2}} \qquad (15)$$

with $n = 0, 1, 2, \cdots$ and K_n the nth-order modified Bessel function of the second kind. $\gamma_{t,1}$ and $\gamma_{t,2}$ are defined by similar expressions as in (9).

The authors verified their method for a dielectric fiber ($\mu_{r,t,1} = \mu_{r,l,1} = 1$) with radius $a = 0.29718$ cm and $\varepsilon_{r,t,1} = 2.55$ located in free space for $\varepsilon_{r,l,1} = 2.55$ and $\varepsilon_{r,l,1} = 2$ at a frequency $f = 42$ GHz. The fiber is approximated by a regular polygon with the same area as the fiber. Table I presents results for the 4 modes above cut off at 42 GHz (Optical nomenclature: HE_{11} ($n = 1$), TE_{01} ($n = 0$), TM_{01} ($n = 0$), and HE_{21} ($n = 2$)) for a polygon with 6 and 8 sides and with 2, 3, and 4 discretization segments on each side. The results are compared with exact solutions obtained with (14). A reasonable accuracy of at least 0.5% is obtained for a hexagon with two segments on each side. Remark that the anisotropy of the permittivity has no influence on the TE_{01} mode which has no longitudinal electric field component.

B. Rib Waveguide

Fig. 3(a) respectively, Fig. 3(b) shows the real, respectively, imaginary part of β/k_0 of the E_{11}^z mode of a dielectric rib waveguide [inset of Fig. 3(a)] as a function of the width w of the waveguide. The structure is isotropic and analyzed at a frequency of 30 GHz and hence a free space wavelength $\lambda_0 = 2\pi/k_0 \cong 1$ cm. Results are found to be in good agreement with results obtained in [3]. Remark that the maxima and dips in the imaginary part due to leakage and cancellation phenomena are found back at the same values of w as in [3].

In Fig. 4 the authors analyzed the same rib waveguide as above, with $w = 2.5\lambda_0$, as a function of the longitudinal permittivity $\varepsilon_{r,l}$ of the waveguide while the relative transversal permittivity was kept at 2.8224. They considered two modes: E_{11}^y and E_{11}^z. The E_{11}^y mode, which is above cut off ($\mathrm{Im}(\beta) = 0$), is almost not influenced by the variation of $\varepsilon_{r,l}$ because this mode has almost no longitudinal electric field component. $\mathrm{Re}(\beta/k_0)$ of the E_{11}^z mode on the other hand increases strongly when $\varepsilon_{r,l}$ increases. At $\varepsilon_{r,1} \cong 4.75$ the propagation constant of the E_{11}^z mode becomes equal to the propagation constant of the TE_0 mode of the underlaying layered medium (also shown on Fig. 4). At this point, the E_{11}^z mode comes above cut off and β/k_0 becomes real. Notice a small coupling effect at this point. At $\varepsilon_{r,l} \cong 7.5$ the lines of the propagation constants of the E_{11}^z and E_{11}^y mode cross. This means that the coupling between the two modes is negligibly small. If the two modes would have coupled the lines of the propagation constants would not cross but would bend away from each other.

In a next step the authors investigated the influence of the conductivity of the semi-infinite bottom layer on the propagation constant of the lowest order mode, i.e., on E_{11}^y. For this purpose, the authors increased the loss tangent $\mathrm{tg}\delta$ of the semi-infinite bottom layer from zero to infinity. Hence, the complex dielectric constant of the semi-infinite layer was selected to be $2.1904(1 - j\mathrm{tg}\delta)$. The width of the rib waveguide was fixed at $w = 2\lambda_0$. The complex propagation constant as a function of $\log(\mathrm{tg}\delta)$ is shown on Fig. 5. The authors start for $\mathrm{tg}\delta = 0$ with the E_{11}^y mode with $\beta/k_0 = 1.61520$. When $\mathrm{tg}\delta$ increases the real part of β/k_0 does not change much and the imaginary part of β/k_0 increases proportional with $\mathrm{tg}\delta$. In the transition region ($0.1 < \mathrm{tg}\delta < 100$) the real part of β drops suddenly and the imaginary part goes through a maximum. In this region

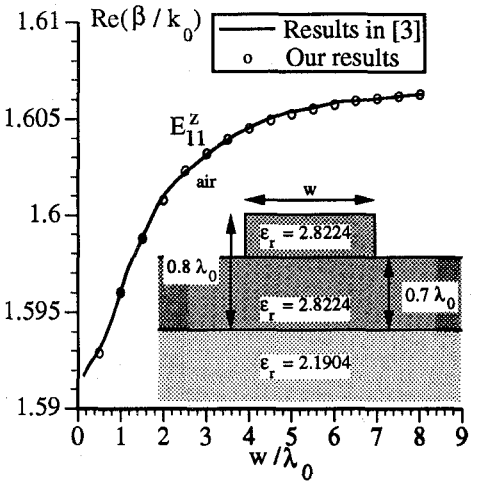

(a)

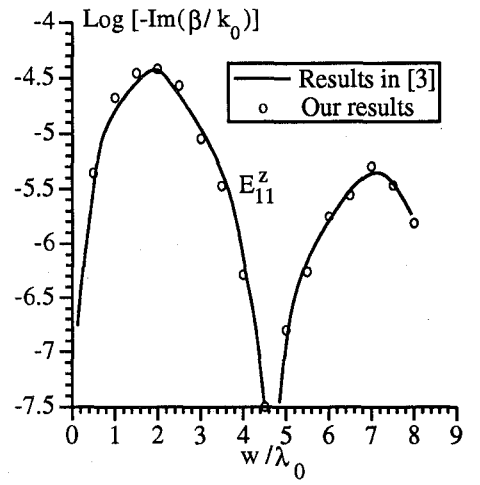

(b)

Fig. 3 (a) Real part of the propagation constant of the E_{11}^z mode of the dielectric rib waveguide, shown on the inset, at 30 GHz and as a function of the width w. (b) Imaginary part of the propagation constant of the E_{11}^z mode of the dielectric rib waveguide shown on the inset of (a), at 30 GHz and as a function of the width w.

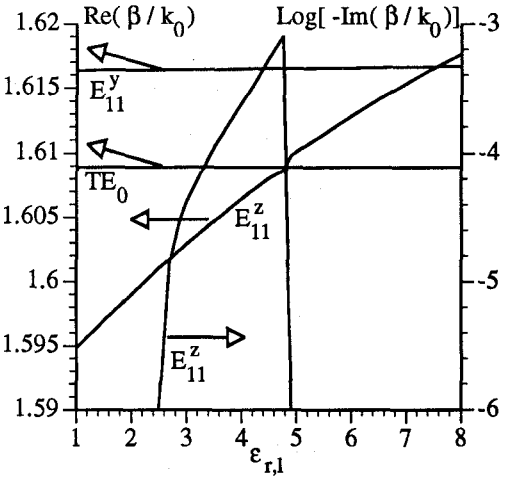

Fig. 4. Real and imaginary part of the propagation constants of the E_{11}^y and E_{11}^z mode at 30 GHz as a function of the longitudinal dielectric constant $\varepsilon_{r,l}$ of the waveguide for the rib waveguide on the inset of Fig. 3(a) with $w = 2.5\lambda_0$.

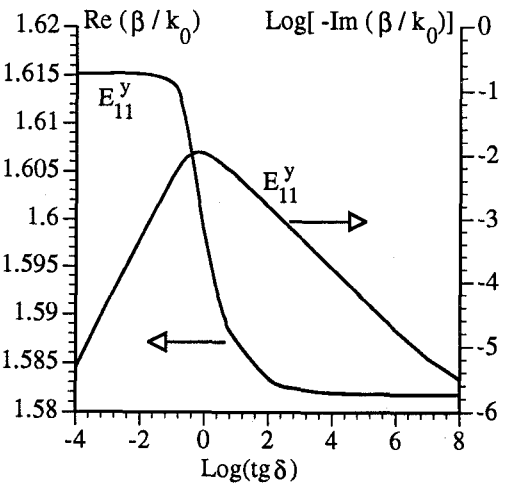

Fig. 5. Real and imaginary part of the propagation constant of the E_{11}^y mode at 30 GHz as a function of loss tangent tgδ of the semi infinite bottom layer of the rib waveguide on the inset of Fig. 3(a) with $w = 2\lambda_0$.

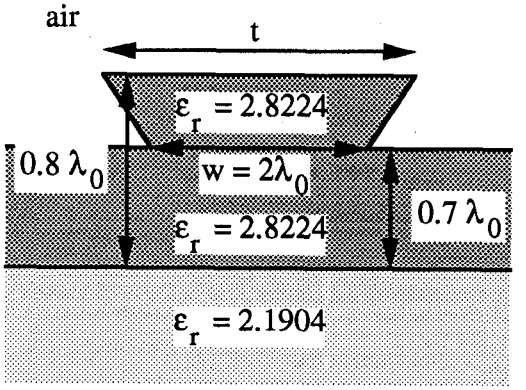

Fig. 6. Geometry of a dielectric rib waveguide with trapezoidal cross-section.

the fields are pushed out of the semi-infinite layer. When tgδ further increases, the real part of β/k_0 remains again almost constant and the imaginary part of β/k_0 decreases proportional with tgδ. The final situation is this where the bottom layer is perfectly conducting. In that case, the imaginary part of β/k_0 becomes zero and $\beta/k_0 = 1.58179$.

Finally, in Fig. 6 the authors start again from the original rib waveguide of Fig. 3(a) but we now selected a trapezoidal cross section for the waveguide. The bottom width w is kept at 2 λ_0 and the top width t is changed from 0 to 4 λ_0. Fig. 7 shows the evolution of the complex propagation constant of the E_{11}^z mode.

C. Strip Dielectric Waveguide

The geometry and parameters of the analyzed strip dielectric waveguide are shown on Fig. 8. Fig. 9(a) shows the real part and Fig. 9(b) shows the imaginary part of the propagation constants of the five lowest modes when the frequency is varied from 0 up to 75 GHz. The results are found to be in excellent agreement with results in [3]. The only difference between the authors results and those in [3] resides in the fact that they found a smooth curve without a dip (see enlargement on the right Fig. 9(b)) for the imaginary part of β/k_0 of

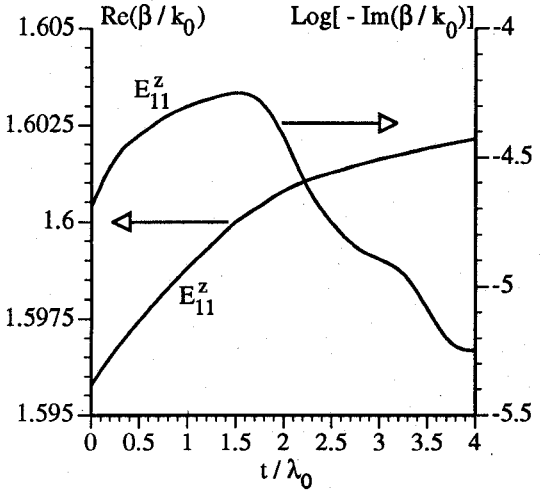

Fig. 7. Real and imaginary part of the propagation constant of the E_{11}^z mode at 30 GHz as a function of the top width t for the rib waveguide of Fig. 6 with $w = 2\lambda_0$.

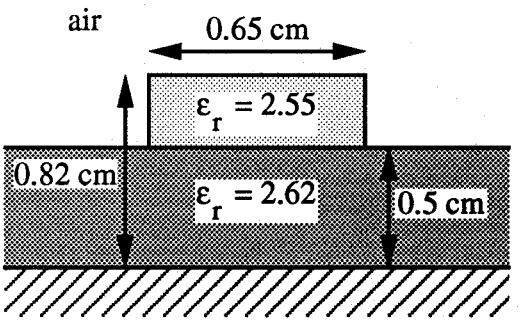

Fig. 8. Geometry of a strip dielectric waveguide.

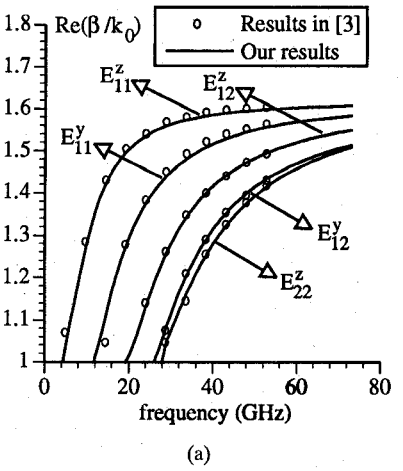

(a)

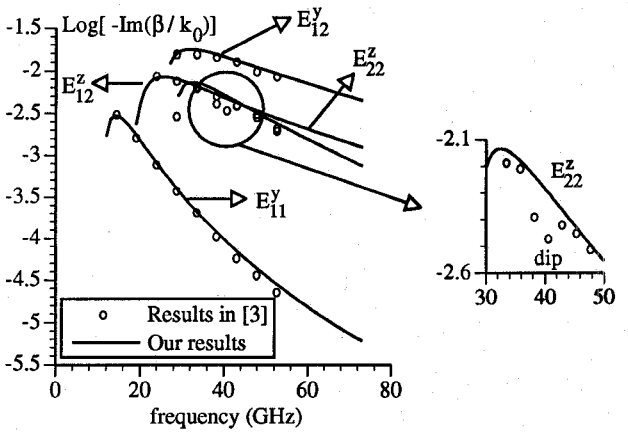

(b)

Fig. 9. (a) Real part of the propagation constants of the lowest five modes of the structure of Fig. 8 when the frequency is varied from 0 up to 75 GHz. (b) Imaginary part of the propagation constants of the lowest five modes of the structure of Fig. 8 when the frequency is varied from 0 up to 75 GHz.

the E_{22}^z mode. The authors believe that their result is more accurate because the other curves on Fig. 9(b) are also smooth and because the dip in [3] remains unexplained.

As a next example, the authors studied the transition from the strip dielectric waveguide of Fig. 8 to a perfectly conducting microstrip by changing the $\mathrm{tg}\delta$ of the waveguide region from zero to infinity. The evolution of the complex propagation constant of the lowest order mode is shown on Fig. 10. The authors start in region 1 with the E_{11}^z mode above cut off at $\mathrm{tg}\delta = 0$. When $\mathrm{tg}\delta$ increases, the real part of β/k_0 remains almost constant and the imaginary part of β/k_0 increases proportionally with $\mathrm{tg}\delta$. From $\mathrm{tg}\delta = 0.1$ on, the fields are pushed out of the waveguide into the air and the real part of β/k_0 decreases. At this point, the imaginary part does not increase any further. At the right side of Fig. 10, in region 3, the authors start with the quasi-TEM mode of the microstrip. The imaginary part of β/k_0 increases proportionally with the decrease of $\mathrm{tg}\delta$. The fields start to penetrate inside the conductor. When $\mathrm{tg}\delta$ decreases further, the real part of β/k_0 starts to increase because the fields see a higher dielectric constant inside the waveguide. At $\mathrm{tg}\delta \approx 40$ the real part of β/k_0 starts to decrease again. The authors think that this is due to the fact that the mode is disappearing. Indeed the quasi-TEM mode cannot exist when $\mathrm{tg}\delta = 0$ because electric field lines cannot originate from a dielectric, while it is precisely for the quasi-TEM mode that the transversal electric field lines start inside the waveguide and go to the ground plane. In the transition region 2 the authors found a whole set of modes with closely spaced propagation constants. The figure shows the real and imaginary part of the propagation constant of one such mode. They lost track of the E_{11}^z mode and the quasi-TEM mode in this region. The authors think that the mode concept loses significance inside this region.

Finally, Fig. 11 shows the propagation constant of the E_{11}^z mode of the strip dielectric waveguide of Fig. 8 when gain is introduced in the waveguide. The gain is characterized by a negative loss tangent. Hence the complex relative permittivity of the waveguide is given by $2.55(1 - j\mathrm{tg}\delta)$ with $\mathrm{tg}\delta < 0$. If the dimensions of the structure and at the same time the frequencies are scaled to optical dimensions and frequencies, then the structure can be a model for a semiconductor laser. Notice the proportional increase of the imaginary part of β/k_0 with the increase of $-\mathrm{tg}\delta$.

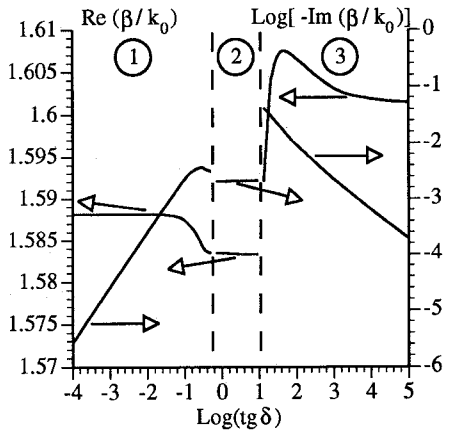

Fig. 10. Real and imaginary part of the propagation constant of the lowest order mode at 42 GHz as a function of the loss tangent $\mathrm{tg}\delta$ of the waveguide of Fig. 8. Region 1: E_{11}^z mode. Region 2: transition region. Region 3: quasi-TEM mode.

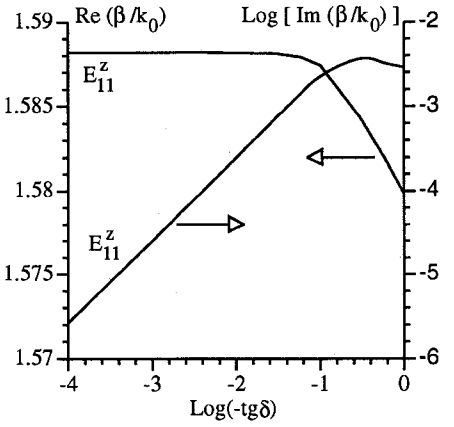

Fig. 11. Real and imaginary part of the propagation constant of the E_{11}^z mode at 42 GHz as a function of the gain (characterized by $-\mathrm{tg}\delta$) of the waveguide of Fig. 8.

REFERENCES

[1] F. Olyslager, D. De Zutter, and K. Blomme, "Rigorous analysis of the propagation characteristics of general lossless and lossy multiconductor transmission lines in multilayered media," *IEEE Trans. Microwave Theory Tech.,* vol. MTT-41, no. 1, pp. 79–88, Jan. 1993.

[2] N. Faché, F. Olyslager, and D. De Zutter, *Electromagnetic and Circuit Modeling of Multiconductor Transmission Lines.* Oxford: Clarendon Press, Oxford Engineering Serils. 35 1993.

[3] J. F. Kiang, S. M. Ali, and J. A. Kong, "Integral equation solution to the guidance and leakage properties of coupled dielectric strip waveguides," *IEEE Trans. Microwave Theory Tech.,* vol. MTT-38, pp. 193–203, Feb. 1990.

[4] Working Group I, COST 216, "Comparison of different modelling techniques for longitudinal invariant integrated optical waveguides," *IEEE Proceedings,* vol. 136, Pt. J, pp. 273–280, Oct. 1989.

[5] K. Hyata, M. Koshiba, M. Egushi, and M. Suzuki, "Vectorial finite-element method without any spurious solutions for dielectric waveguide problems using transverse magnetic-field component," *IEEE Trans. Microwave Theory Tech.,* vol. MTT-34, pp. 1120–1124, Nov. 1986.

[6] E. W. Kolk, N. H. G. Baken, and H. Blok, "Domain integral equation analysis of integrated optical channel and ridge waveguides in stratified media," *IEEE Trans. Microwave Theory Tech.,* vol MTT-38, pp. 78–85, Jan. 1990.

[7] N. Faché, F. Olyslager, and D. De Zutter, "Full-wave analysis of coupled perfectly conducting wires in a multilayered medium," *IEEE Trans. Microwave Theory Tech.,* vol. MTT-39, pp. 673–681, April 1991.

[8] M. Abramowitz and I. A. Stegun, *Handbook of Mathematical Functions with Formulas, Graphs and Mathematical Tables.* New York: Dover, 1970.

[9] N. Faché, J. Van Hese, and D. De Zutter, "Generalized space domain Green's dyadic for multilayered media with special application to microwave interconnections," *J. Electromagn. Waves and Appl.,* vol. 3, pp. 651–669, 1989.

[10] L. B. Felsen and N. Marcuvitz, *Radiation and Scattering of Waves,*. Englewood Cliffs, New Jersey: Prentice-Hall, 1973.

[11] R. E. Collin, *Field Theory of Waves.* New York: McGraw-Hill Company, 1960.

[12] K. A. Michalski and D. Zheng, "Analysis of microstrip resonators of arbitrary shape," *IEEE Trans. Microwave Theory Tech.,* vol. MTT-40, pp. 112–119, Jan. 1992.

[13] T. Okoshi, *Optical Fibers.* New York: Academic, 1982.

Daniël De Zutter was born in Eeklo, Belgium on November 8, 1953. He received a degree in electrical engineering from the University of Ghent in July 1976. From September 1976 to September 1984 he was a research and teaching assistant in the Laboratory of Electromagnetism and Acoustics (LEA) at the same university. In October 1981, he obtained the Ph.D. degree at the University of Ghent and in the spring of 1984 he completed a thesis leading to a degree equivalent to the French Aggrégation or the German Habilitation. He is now a professor at Ghent University and Research Director at the National Science Foundation of Belgium.

Most of his earlier scientific work dealt with the electrodynamics of moving media, with emphasis on the Doppler effect and Lorentz forces. His research now focusses on all aspects of circuit and electromagnetic modelling of high-speed and high-frequency interconnections and on EMC and EMI topics. He has contributed to more than 30 jounal papers and about 40 conference papers. In 1990 he was elected Member of the Electromagnetics Society.

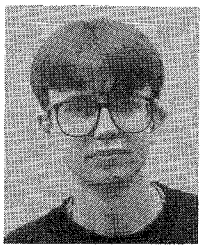

Frank Olyslager was born in Wilrijk, Belgium, on November 24, 1966. He received a degree *summa cum laude* in electrical engineering at the University of Ghent in July 1989. He received the Ph.D. degree in electrical engineering at the Laboratory of Electromagnetism and Acoustics of the University of Ghent in February 1993. At present he is a Research Assistant of the National Fund for Scientific Research of Belgium.

His research concerns the use of integral equation techniques to solve Maxwell's equations numerically. His activities focus on the electromagnetic wave propagation on high-frequency electrical and optical interconnections in multilayered media.